**SUPPLEMENT**

## SUPPLEMENTARY TABLES

**Table 1. Legend of BASE immune cell type and their descriptions**

| Cell Name | ImmGen Labels | Comments |
|---|---|---|
| CD8+ T cell -1 | T.8EFF.SP.OT1.12HR.LISOVA | CD8+ T Cell |
| NK cell | NK.Hpos.MCMV1.SP | NK cell signature |
| T cell -1 | TGD.TH | $\gamma\delta$ T cell signature |
| GD T cell -2 | IMMTGD.VG2.E17.TH | Immature $\gamma\delta$ T cell signature |
| T cell -3 | NKT.44negNK1.1neg.TH | Natural Killer T Cell signature |
| CD4+ T Cell -2 | T.4MEM.SP | CD4+ Memory T Cell |
| Macrophage-1 | DC.103pos11Bneg.SALM3.SI | Small intestine monocyte signature |
| Macrophage-2 | DC7.LN | Lymph node monocyte signature |
| Macrophage-3 | DC.103neg11Bpos.LV | Live monocyte signature |
| Macrophage-4 | MF.THIO5.IIpos480INT.PC | Peritoneal cavity macrophage |
| B cell -1 | B.FO.LN | B cell found in lymph node |
| B cell -2 | B.FO.PC | B cell in peritoneal cavity signature |
| pDC | DC.PDC.8pos.MLN | Active dendritic cell with a plasmocytoid dendritic cell signature |

**Table S2. Cox regression results from backward selection performed on LASSO predictors.** We performed backward selection on LASSO predictors, which are predictive of metastasis status, in order to determine influence of immune infiltration scores on overall survival. Of the 13 LASSO predictors, three immune infiltration scores as well as age were considered significant predictors of overall survival in the TCGA cohort. These three immune infiltration scores served as inputs for the cox-proportional hazards model.

| Immune Predictors | HR | Lower 95% CI | Upper 95% CI | p- value |
|---|---|---|---|---|
| **CD8+ T cell-1** | 1.0289 | 1.0002 | 1.058 | 0.0484 |
| **CD4+ T cell-2** | 1.0565 | 1.0140 | 1.100 | 0.0086 |
| **DC Active** | 0.9262 | 0.8828 | 0.971 | 0.0017 |
| **Age** | 1.0274 | 1.0115 | 1.011 | 0.00069 |

**N=** 376
**Number of events =** 112
Concordance = 0.661 (SE = 0.03)
Predictive Model was compared to the null model ($H_0$: Age + Sex ≠ 0)
Log-liklihood: -558.22
Chisq: 27.357
Df = 2, p = $1.147*10^{-06}$

**Table S3. Comparison of CIBERSORT immune fractions between M0 and M1 tumors.** We compared filtered ($p < 0.05$) CIBERSORT immune fractions of 22 immune cell types in M0 and M1 tumors using a wilcox-rank sum test (FDR adjusted). CD4+ Memory activated T cell, CD8+ T cell, and activated dendritic cell immune fractions differed between M0 and M1 RCC tumors.

| CIBERSORT Cell Type | FDR Q-Value |
|---|---|
| B.cells.naive | 0.272017555 |
| B.cells.memory | 0.02201098 |
| Plasma.cells | 0.067387964 |
| T.cells.CD8 | 3.55E-05 |
| T.cells.CD4.naive | 0.496861598 |
| T.cells.CD4.memory.resting | 0.027850892 |
| T.cells.CD4.memory.activated | 0.00152955 |
| T.cells.follicular.helper | 0.006934386 |
| T.cells.regulatory..Tregs. | 0.00152955 |
| T.cells.gamma.delta | 0.837012719 |
| NK.cells.resting | 0.012198799 |
| NK.cells.activated | 0.128604188 |
| Monocytes | 0.431883305 |
| Macrophages.M0 | 0.272000094 |
| Macrophages.M1 | 0.019997535 |
| Macrophages.M2 | 0.002126874 |
| Dendritic.cells.resting | 0.364655006 |
| Dendritic.cells.activated | 0.007087499 |
| Mast.cells.resting | 0.001794244 |
| Mast.cells.activated | 0.107804894 |
| Eosinophils | 0.107804894 |
| Neutrophils | 0.107804894 |

**Table S4. Cox-proportional hazard modeling with CIBERSORT immune fractions.** Using the 22 immune cell type fractions generated from CIBERSORT, we implemented age and sex adjusted Cox-proportional hazard modeling only on cell types which also associated with survival in the BASE outputs. Here we highlight CD8+ T cell, and CD4+ T cell memory activated, and activated dendritic cells are associated with survival.

| CIBERSORT Cell Type | HR | Lower 95% CI | Upper 95% CI | FDR Q value |
|---|---|---|---|---|
| **T.cells.CD8** | 53.81005 | 4.5657318 | 634.185642 | 0.011088 |
| **T.cells.regulatory.Tregs.** | 3.49E+04 | 6.4224001 | 1.83E+07 | 0.011088 |
| **Mast.cells.resting** | 0.000124 | 1.31E-07 | 0.1183589 | 0.02693863 |
| **Macrophages.M2** | 0.00855 | 0.000121078 | 0.6033704 | 0.05133333 |
| **T.cells.follicular.helper** | 2.72E+04 | 74.1532079 | 9.95E+06 | 0.011088 |
| **Dendritic.cells.activated** | 2.75E-13 | 2.81E-21 | 2.69E-05 | 0.011088 |
| **NK.cells.resting** | 0.03492 | 3.88E-05 | 31.418187 | 0.40044 |
| **Macrophages.M1** | 7.36E+07 | 2040.01438 | 2.66E+12 | 0.011088 |
| **B.cells.memory** | 5.513 | 5.83E-06 | 5.22E+06 | 0.8079 |
| **T.cells.CD4.memory.resting** | 0.00842 | 0.000350989 | 0.2020249 | 0.01173333 |
| **T.cells.CD4.memory.activated** | 1.18E+11 | 1.8749344 | 7.45E+21 | 0.06526656 |
| **Plasma.cells** | 0.004415 | 3.22E-05 | 0.606 | 0.04623 |

**Table S5. GSEA enrichment of immune signatures comparing M0 and M1 RCC tumors.** GSEA analysis was performed on RNA-Seq data from RCC tumors to compare RCC M0 vs. RCC M1 tumors to determine enrichment of immunological signatures obtained from the MSigDB database (C7). Compared to M0, M1 tumors were enriched for 115 immunological signatures, of which the top 10 (based on the FDR-corrected Q-value) are presented here. There was no enrichment of immunological signatures in M0 RCC tumors compared to M1. Of the top 10 pathways enriched in M1 RCC tumors, most (7/10) are pathways known to be typically downregulated when comparing naïve T cells to differentiated T cell states. Suggesting T cells in M1 RCC tumors have a well-differentiated phenotype.

| Name | Size | NES | Nominal p-value | FDR Q-value | Relevance/ Comments |
|---|---|---|---|---|---|
| **GSE3982_NEUTROPHIL_VS_TH1_DN** | 175 | -1.544 | 0.081 | 0.202 | Genes downregulated in comparison of neutrophils and Th1 cells |
| **GSE17974_0H_VS_72H_IN_VITRO_ACT_CD4_TCELL_DN** | 181 | -1.545 | 0.064 | 0.202 | Genes downregulated in comparison of untreated CD4 T cells at 0 h vs. 72 hr |
| **GSE12845_NAIVE_VS_PRE_GC_TONSIL_BCELL_DN** | 184 | -1.545 | 0.081 | 0.205 | Genes downregulated in comparison of naïve B cell versus pre-germinal tonsil B cells |
| **GSE36476_CTRL_VS_TSST_ACT_40H_MEMORY_CD4_TCELL_YOUNG_DN** | 178 | -1.547 | 0.041 | 0.206 | Genes downregulated in comparison of untreated CD4 memory T cells vs. CD4 T cells treated with TSST at 40 hr. |
| **GSE22886_NAIVE_CD4_TCELL_VS_48H_ACT_TH1_DN** | 180 | -1.547 | 0.064 | 0.209 | Genes downregulated in comparison of naïve CD4 vs. stimulated CD Th1 cells at 48 hr. |
| **GSE28726_NAIVE_VS_ACTIVATED_CD4_TCELL_DN** | 187 | -1.557 | 0.042 | 0.209 | Genes downregulated in CD4 T cells: naïve vs. activated |
| **GSE24634_TEFF_VS_TCONV_DAY7_IN_CULTURE_UP** | 184 | -1.559 | 0.041 | 0.209 | Genes upregulated in CD25+ T effector cells vs. CD25- T cells |
| **GSE22589_HEALTHY_VS_HIV_AND_SIV_INFECTED_DC_UP** | 163 | -1.560 | 0.056 | 0.210 | Genes up-regulated in monocyte-derived dendritic cells (control vs. HIV and SIV infection) |
| **GSE25085_FETAL_LIVER_VS_ADULT_BM_SP4_THYMIC_IMPLANT_UP** | 161 | -1.548 | 0.052 | 0.211 | genes upregulated in thymic implants from fetal liver vs. adult bone marrow |
| **GSE2770_TGFB_AND_IL4_VS_IL12_TREATED_ACT_CD4_TCELL_6H_DN** | 172 | -1.494 | 0.056 | 0.211 | Genes down-regulated in CD4 T cells activated by anti-CD28 and anti-CD3 |

**Table S6**. **Immune checkpoint marker expression and CD8+ T cell infiltration in TCGA cohort.** The association between immune checkpoint markers and CD8+ T cell-1infiltration was examined using regression models, which adjust for age, sex, and tumor purity (as assessed by the ABSOLUTE algorithm). We examined the association between PDCD1, CTLA4, CD38, and TIGIT and the interaction between CD8+ T cell-1 infiltration and metastasis status.
$Model\ (M)$: $E[g] = \hat{\beta}_1 IS_{CD8+} + \hat{\beta}_2 M + \hat{\beta}_3 IS_{CD8+} * M + \hat{\beta}_4 P_{ABSOLUTE} + \hat{\beta}_5 s + \hat{\beta}_6 a$ , where $E[g]$ is the log10 normalized gene expression of PDCD1, CTLA4, TIGIT, and CD38, and $IS_{CD8+}$ is the CD8+ T cell-1 infiltration score, $M$ is metastasis status, $S$ is sex, $A$ is age, and $P_{ABSOLUTE}$ is the purity score generated from the absolute algorithm. Note, SE is the standard error.

| Outcome | Predictor | $\widehat{\boldsymbol{\beta}}$ | SE | p-value |
|---|---|---|---|---|
| $\boldsymbol{M1: E[g] \sim PDCD1}$ | $IS_{CD8+}$ | 0.0217 | 0.00413 | $2.62*10^{-07}$ |
| | $M$ | -0.176 | 0.167 | 0.293 |
| | $IS_{CD8+} * M$ | 0.0180 | 0.0103 | 0.0816 |
| | $P_{ABSOLUTE}$ | -1.36 | 0.210 | $4.02*10^{-10}$ |
| | $s$ | -0.0135 | 0.0645 | 0.834 |
| | $a$ | -0.0192 | 0.00251 | 0.443 |
| | | | | |
| $\boldsymbol{M2: E[g] \sim CTLA4}$ | $IS_{CD8+}$ | 0.0141 | 0.00380 | 0.000254 |
| | $M$ | -0.178 | 0.153 | 0.246 |
| | $IS_{CD8+} * M$ | 0.0198 | 0.00949 | 0.0381 |
| | $P_{ABSOLUTE}$ | -1.30 | 0.193 | $7.54*10^{-11}$ |
| | $s$ | -0.0247 | 0.0593 | 0.676 |
| | $a$ | -0.000280 | 0.00231 | 0.903 |
| | | | | |
| $\boldsymbol{M3: E[g] \sim TIGIT}$ | $IS_{CD8+}$ | 0.0123 | 0.00386 | 0.00157 |
| | $M$ | -0.257 | 0.156 | 0.1006 |
| | $IS_{CD8+} * M$ | 0.0223 | 0.00964 | 0.02119 |
| | $P_{ABSOLUTE}$ | -1.38 | 0.196 | $1.29*10^{-11}$ |
| | $s$ | 0.0269 | 0.0602 | 0.655 |
| | $a$ | -0.00182 | 0.00234 | 0.436 |
| | | | | |
| $\boldsymbol{M4: E[g] \sim CD38}$ | $IS_{CD8+}$ | 0.00863 | 0.00329 | 0.00917 |
| | $M$ | -0.191 | 0.133 | 0.153 |
| | $IS_{CD8+} * M$ | 0.0179 | 0.00822 | 0.02956 |
| | $P_{ABSOLUTE}$ | -1.78 | 0.00200 | $1.33*10^{-11}$ |
| | $s$ | 0.00118 | 0.0514 | 0.981 |
| | $a$ | -0.000717 | 0.00200 | 0.720 |
| | | | | |

**Table S7. Enrichment of oncogenic signatures in M1 compared to M0 RCC tumors.** GSEA was used to compare the normalized enrichment scores (NES) of oncogenic signatures obtained from the MSigDB database (C6) between M0 and M1 tumors. M1 tumors were enriched for seven oncogenic signatures, based on the FDR-corrected Q-value.

| Name | Size | NES | Nominal p-value | FDR Q-value | Relevance/Comments |
|---|---|---|---|---|---|
| LEF1_UP.V1_DN | 170 | -1.793 | 0.0001 | 0.088 | Genes down-regulated in colon carcinoma; over-expression of LEF1 results in EMT induction within 48 hours |
| CSR_LATE_UP.V1_UP | 155 | -1.507 | 0.048 | 0.176 | |
| RPS14_DN.V1_DN | 161 | -1.598 | 0.006 | 0.186 | Genes downregulated in CD34+ hematopoietic cells in RPS14 knockdown |
| SIRNA_EIF4GI_UP | 86 | -1.512 | 0.074 | 0.197 | |
| P53_DN.V1_UP | 180 | -1.630 | 0.017 | 0.220 | Genes up-regulated with mutated p53 |
| BCAT_GDS748_UP | 48 | -1.513 | 0.028 | 0.233 | Genes up-regulated in kidney fibroblasts with active CTNNB1 |
| SINGH_KRAS_DEPENDENCY_ SIGNATURE_ | 19 | -1.536 | 0.008 | 0.240 | Genes defining KRAS signatures |

**Table S8. Cox-Model for SENESCENCE_TP53_TARGETS_DN in TCGA dataset:** Survival model examining the effect of senescence SENESENCE_TP53_TARGETS_DN enrichment on overall survival in the TCGA cohort, while adjusting for age, sex, and metastasis status.

| SENESCENCE_TP53_DN Model | HR | Lower 95% CI | Upper 95% CI | p- value |
|---|---|---|---|---|
| SENESCENCE_TP53_TARGETS_DN | 15.60315 | 2.3922 | 101.772 | 0.00408 |
| AGE | 1.033679 | 1.0155 | 1.052 | 0.00025 |
| SEX | 1.147110 | 0.7763 | 1.695 | 0.4908 |
| Metastasis Status | 6.40265 | 4.2894 | 9.557 | $<2*10^{-16}$ |
| **N=** 376<br>**Number of events =** 112<br>Concordance = 0.799 (SE = 0.953)<br>Likelihood Ratio Test = 113.6 on 4 df, p=0<br>Wald test = 113.8 on 4 df, p=0<br>Score (logrank) = 151.1 on 4 df, p=0 | | | | |

**Table S9. The effect of SENESCENCE_TP53_DN on overall survival in the immunotherapy dataset.** The effect of SENESCENCE_TP53_TARGETS_DN on overall survival was examined using cox proportional hazards modeling while adjusting for age, sex, and cohort status (discovery vs. validation).

| SENESCENCE_TP53_DN Model | HR | Lower 95% CI | Upper 95% CI | p- value |
|---|---|---|---|---|
| SENESCENCE_TP53_TARGETS_DN | 0.003775 | $1.625*10^{-05}$ | 0.8772 | 0.0447 |
| AGE | 0.969811 | 0.9082 | 1.0356 | 0.3598 |
| SEX | 1.670602 | 0.565 | 4.9398 | 0.3535 |
| COHORT STATUS | 1.031191 | 0.4189 | 2.5382 | 0.9467 |
| **N=** 33<br>**Number of events =** 23<br>Concordance = 0.683 (SE = 0.073)<br>Likelihood Ratio Test = 5.2 on 4 df, p=0.2676<br>Wald test = 4.48 on 4 df, p=0.3451<br>Score (logrank) = 4.45 on 4 df, p=0.3381 | | | | |

**Table S10. Extended Table 2: TP53-inactivation induced senescence differentially influences the tumor microenvironment in M0 and M1 tumors.** Below is an extended version of Table 2 from the main manuscript. Effect sizes, standard errors (SE) and p-values for all terms in each regression model (M1-M5) are shown.

| Model | Outcome | Variable | $\widehat{\boldsymbol{\beta}}$ | SE | p-value |
|---|---|---|---|---|---|
| $\boldsymbol{M1}$ | $E[g] \sim$ cGAS | $ES_{senescence\_UP}$ | 1.365 | 0.3475 | 0.000102 |
| | | $M$ | 0.8948 | 0.2211 | $6.36*10^{-05}$ |
| | | $ES_{senescence\_UP} * M$ | -2.714 | 0.7275 | 0.000221 |
| | | $s$ | -0.003368 | 0.03296 | 0.918 |
| | | $a$ | -0.001368 | 0.001276 | 0.284 |
| $\boldsymbol{M2}$ | $E[g] \sim$STING | $ES_{senescence\_UP}$ | 1.660 | 0.2838 | $1.08*10^{-08}$ |
| | | $M$ | 0.5068 | 0.1806 | 0.00530 |
| | | $ES_{senescence\_UP} * M$ | -1.551 | 0.5942 | 0.00941 |
| | | $s$ | -0.08097 | 0.02692 | 0.00281 |
| | | $a$ | 0.0005178 | 0.001042 | 0.619 |
| $\boldsymbol{M3}$ | $E[g] \sim$PRF1 | $ES_{senescence\_UP}$ | 2.397 | 0.5247 | $6.66*10^{-06}$ |
| | | $M$ | 1.047 | 0.3339 | 0.00184 |
| | | $ES_{senescence\_UP} * M$ | -3.236 | 1.098 | 0.00342 |
| | | $s$ | 0.03354 | 0.04976 | 0.501 |
| | | $a$ | -0.001085 | 0.001926 | 0.573 |
| $\boldsymbol{M4}$ | $E[g] \sim$GZMA | $ES_{senescence\_UP}$ | 2.054 | 0.6228 | 0.00106 |
| | | $M$ | 1.060 | 0.3963 | 0.00782 |
| | | $ES_{senescence\_UP} * M$ | -2.930 | 1.303 | 0.0252 |
| | | $s$ | 0.04257 | 0.05906 | 0.471 |
| | | $a$ | 0.0001382 | 0.002286 | 0.951 |
| $\boldsymbol{M5}$ | $E[p] \sim P_{Hypoxia}$ | $ES_{senescence\_UP}$ | 0.7909 | 0.09713 | $5.97*10^{-15}$ |
| | | $M$ | 0.1832 | 0.06182 | 0.00323 |
| | | $ES_{senescence\_UP} * M$ | -0.5865 | 0.2033 | 0.00415 |
| | | $s$ | -0.01824 | 0.009212 | 0.0484 |
| | | $a$ | -0.0006634 | 0.0003566 | 0.0636 |

$M1 - M4$: $E[g] = \hat{\beta}_1 ES_{senescence\_UP} + \hat{\beta}_2 M + \hat{\beta}_3 ES_{senescence\_UP} * M + \hat{\beta}_4 a + \hat{\beta}_5 s$
$M5$: $E[p] = \hat{\beta}_1 ES_{senescence\_UP} + \hat{\beta}_2 M + \hat{\beta}_3 ES_{senescence\_UP} * M + \hat{\beta}_4 a + \hat{\beta}_5 s$ ,
where $E[g]$ is the expected $log_{10}$ normalized gene expression of cGAS (MB21D1), STING, PRF1, or GZMA, $ES_{senescence\_UP}$ is SENESCENCE_TP53_TARGETS_UP pathway enrichment scores, $E[p]$ is the expected pathway enrichment score of $P_{Hypoxia}$, the MANIA_HYPOXIA_VHL_TARGETS_UP pathway, $M$ is metastasis status, $a$ is age, and $s$ is sex.

Note: SE is standard error

**Table S11. Examining predictive effect of senescence immune interactions on immunotherapy response in metastatic melanoma.** Logistic regression modeling was applied to the Hugo et al., 2016 anti-PD-1 dataset (n=25) to determine if senescence immune interactions were predictive of response to anti-PD-1 therapy. irRECIST categories were binned into two categories—Response (Complete Response/Partial Response = 1) and Disease (Progressive Disease = 0) and this is the main outcome in all regression models. We also compared the performance of our senescence-immune models $(M1 - M6)$ to the immunophenotype score (IPS) model $(M7)$. All models $(M1 - M7)$ were adjusted for age and sex and were compared to the null model $(M0)$, which also adjusts for age and sex in order to determine model significance.

| Model | Predictors | $\widehat{\beta}$ | SE | p-value | AIC | Model p-value |
|---|---|---|---|---|---|---|
| $\boldsymbol{M1}$ | $ES_{senesence\_UP}$ | -4.876 | 11.16 | 0.662 | | |
| | $cGAS$ | 99.64 | 513.5 | 0.846 | | |
| | $ES_{senesence\_UP} * cGAS$ | -227.5 | 871.8 | 0.794 | | |
| | | | | | 44.72 | 0.579 |
| $\boldsymbol{M2}$ | $ES_{senesence\_UP}$ | -9.16 | 10.36 | 0.377 | | |
| | $PDCD1$ | -52.06 | 268.1 | 0.846 | | |
| | $ES_{senesence\_UP} * PDCD1$ | 55.73 | 515.4 | 0.914 | | |
| | | | | | 44.37 | 0.502 |
| $\boldsymbol{M3}$ | $ES_{senesence\_UP}$ | -7.371 | 9.616 | 0.443 | | |
| | $PRF1$ | 16.49 | 168.2 | 0.922 | | |
| | $ES_{senesence\_UP} * PRF1$ | -89.36 | 314.9 | 0.777 | 42.23 | 0.216 |
| $\boldsymbol{M4}$ | $ES_{senesence\_UP}$ | -7.119 | 11.90 | 0.550 | | |
| | $GZMA$ | -16.72 | 102.3 | 0.870 | | |
| | $ES_{senesence\_UP} * GZMA$ | -1.402 | 187.9 | 0.994 | | |
| | | | | | 42.44 | 0.236 |
| $\boldsymbol{M5}$ | $ES_{senesence\_UP}$ | -39.57 | 19.97 | 0.047 | | |
| | $STING$ | -101.9 | 91.79 | 0.266 | | |
| | $ES_{senesence\_UP} * STING$ | 219.0 | 159.8 | 0.170 | | |
| | | | | | 37.06 | 0.0220 |
| $\boldsymbol{M6}$ | $ES_{senesence\_DN}$ | -8.267 | 4.357 | 0.0578 | | |
| | | | | | 37.38 | 0.0274 |
| $\boldsymbol{M7}$ | $IPS$ | 0.6974 | 0.4051 | 0.085 | | |
| | | | | | 39.08 | 0.0577 |

$M0\ (Null)$: $logit(P(Y=1) = \hat{\beta}_1 a + \hat{\beta}_2 s$

$M1$: $logit(P(Y=1) = \hat{\beta}_1 a + \hat{\beta}_2 s + \hat{\beta}_3 ES_{senesence\_UP} + \hat{\beta}_4 cGAS + \hat{\beta}_5 ES_{senesence\_UP} * cGAS$

$M2$: $logit(P(Y=1) = \hat{\beta}_1 a + \hat{\beta}_2 s + \hat{\beta}_3 ES_{senesence\_UP} + \hat{\beta}_4 PDCD1 + \hat{\beta}_5 ES_{senesence\_UP} * PDCD1$

$M3$: $logit(P(Y=1) = \hat{\beta}_1 a + \hat{\beta}_2 s + \hat{\beta}_3 ES_{senesence\_UP} + \hat{\beta}_4 GZMA + \hat{\beta}_5 ES_{senesence\_UP} * GZMA$

$M4$: $logit(P(Y=1) = \hat{\beta}_1 a + \hat{\beta}_2 s + \hat{\beta}_3 ES_{senesence\_UP} + \hat{\beta}_4 PRF1 + \hat{\beta}_5 ES_{senesence\_UP} * PRF1$

$M5$: $logit(P(Y=1) = \hat{\beta}_1 a + \hat{\beta}_2 s + \hat{\beta}_3 ES_{senesence\_UP} + \hat{\beta}_4 PDL1 + \hat{\beta}_5 ES_{senesence\_UP} * STING$

$M6$: $logit(P(Y=1) = \hat{\beta}_1 a + \hat{\beta}_2 s + \hat{\beta}_3 ES_{senesence\_DN}$

$M7$: $logit(P(Y=1) = \hat{\beta}_1 a + \hat{\beta}_2 s + \hat{\beta}_3 IPS,$ where $Y=1$ is assosciated with response, $a$ is age, $s$ is sex, $ES_{senesence\_UP}$ is SENESENCE_TP53_TARGETS_UP pathway enrichment score, $ES_{senesence\_DN}$ is SENESENCE_TP53_TARGETS_DN pathway enrichment score, $cGAS\ and\ PDCD1, PRF1, GZMA, and\ STING$ are $log_{10}$ normalized gene expression values for the cGAS and PDCD1, PRF1, GZMA, and STING (TMEM173) genes respectively, and $IPS$ is the immunophenotype score (IPS). All models were compared with the $Null$ model to determine model significance.

Note: SE is standard error and AIC is Akaike Information Criterion

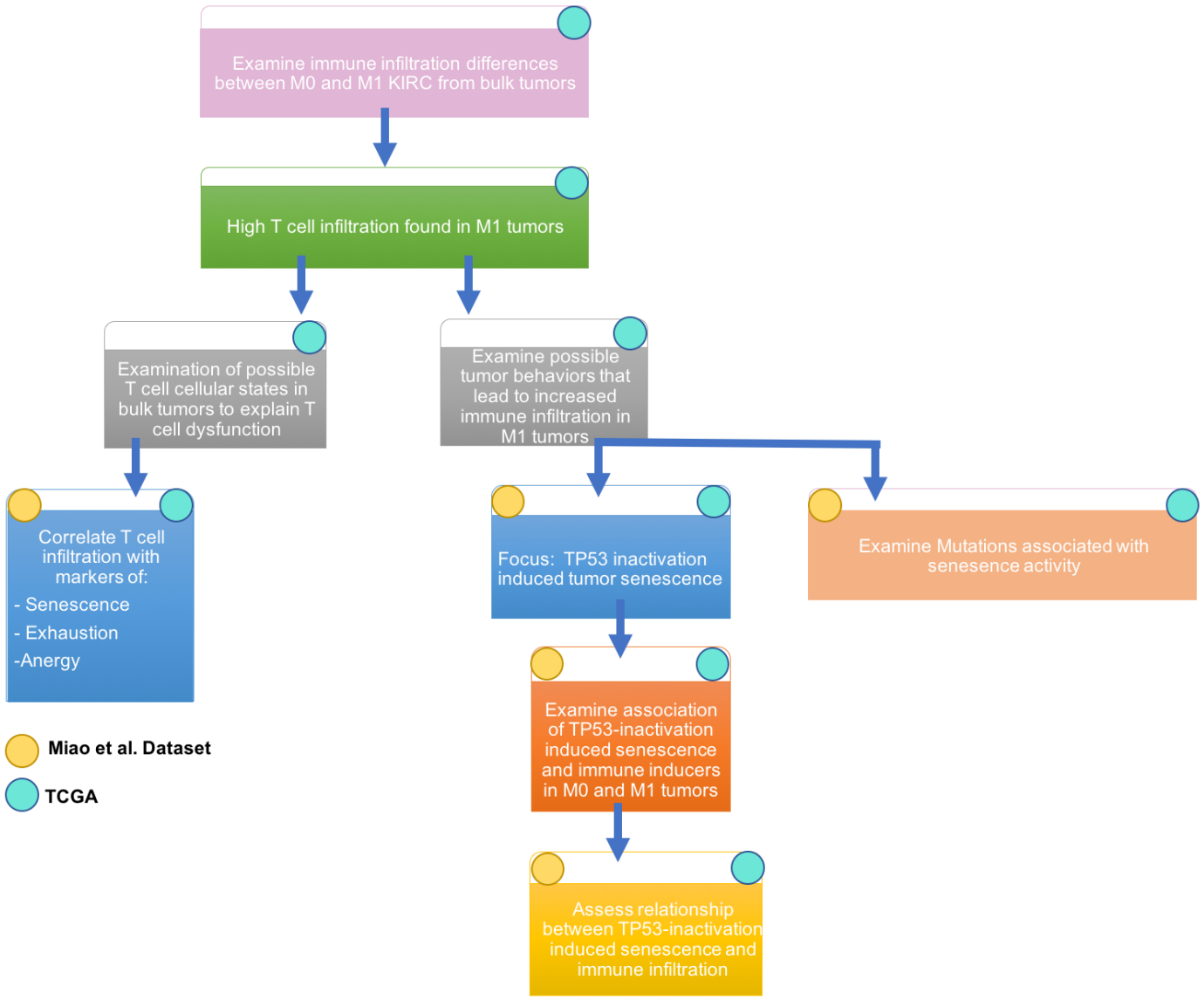


**Figure S1. Conceptual diagram of immune and senescence analysis in TCGA and Miao et al datasets**

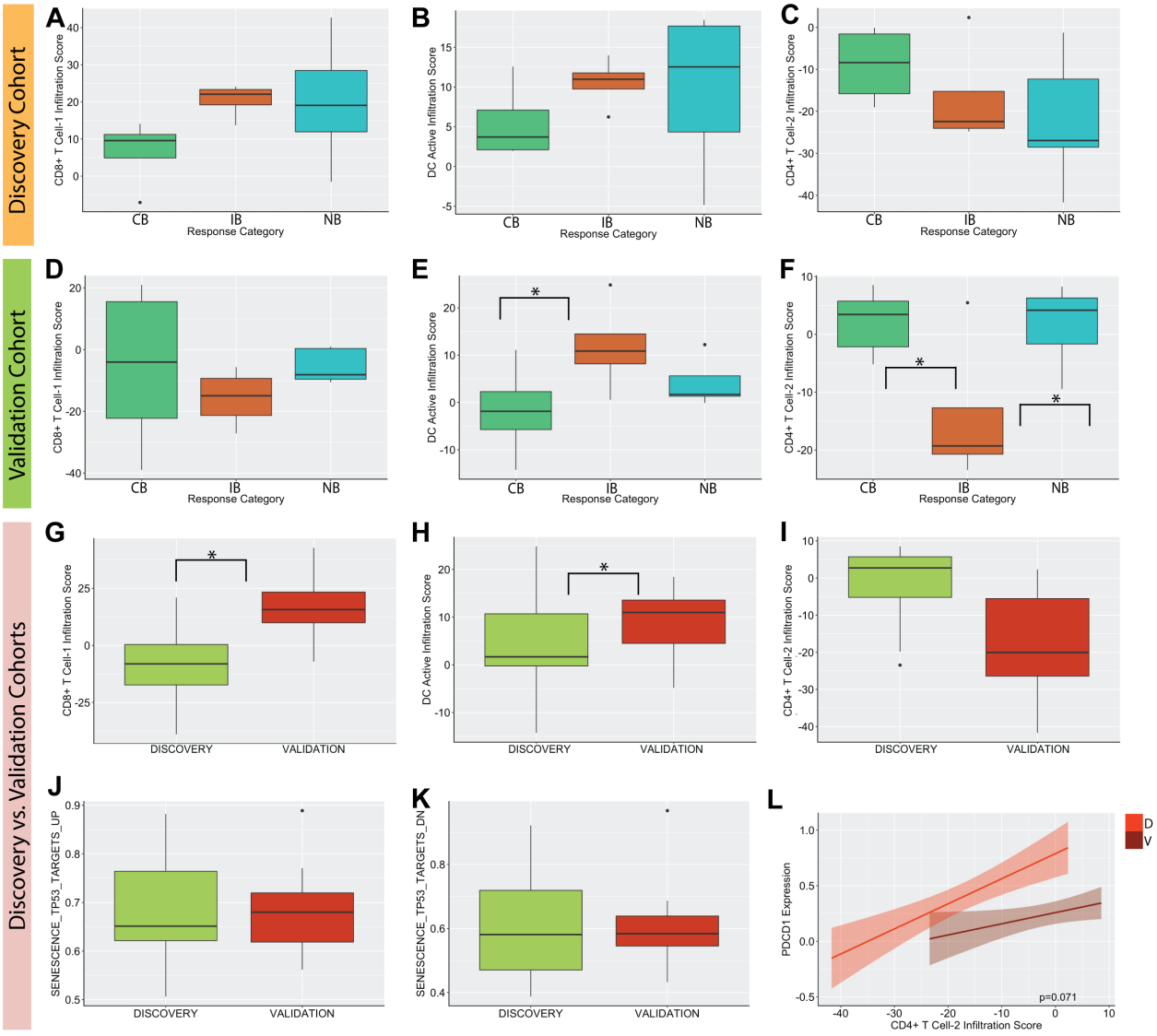


**Figure S2. Tumor immune microenvironment characterization in the discovery and validation cohorts.** Boxplots comparing CD8+ T Cell-1 (A,D), DC Active (B,E), and CD4+ Tcell-2 (C,F) infiltration in the discovery (A-C) and validation (D-F) cohorts are shown. Boxplots comparing CD8+ T cell-1 (G), DC Active (H), and CD4+ Tcell-2 (I) infiltration scores and SENESENCE_TP53_TARGETS_UP (J) and SENESENCE_TP53_TARGETS_DN (K) enrichment scores between the validation and discovery cohorts are also shown. Lastly, we examined the difference in the association of PDCD1 expression and CD4+ T cell-2 infiltration between the discovery and validation cohorts (L).
** = p <0.01, * = p < 0.05, † = p <0.1

**Immune infiltration differences between discovery and validation cohorts**

We note immune infiltration differences between the discovery and validation cohorts obtained from the Miao et al., 2018 dataset. Notably, the validation cohort has higher CD8+ T cell-1 and active dendritic cell (DC Active) tumor infiltration compared to the discovery cohort. Furthermore, in the validation cohort, higher active dendritic cell infiltration is found in tumors from patients who received intermediate benefit to checkpoint blockade therapy compared to a complete benefit. Higher CD4+ T cell-2 infiltration was found in tumors from patients who received complete benefit or no benefit from checkpoint blockade therapy compared to patients who received intermediate benefit from therapy.

Lastly, we note PDCD1 gene expression associates with CD4+ T cell-2 infiltration differently in the discovery cohort compared to the validation cohort. Note, we did not observe any differences in tumor senescence activity between the validation and discovery cohorts.

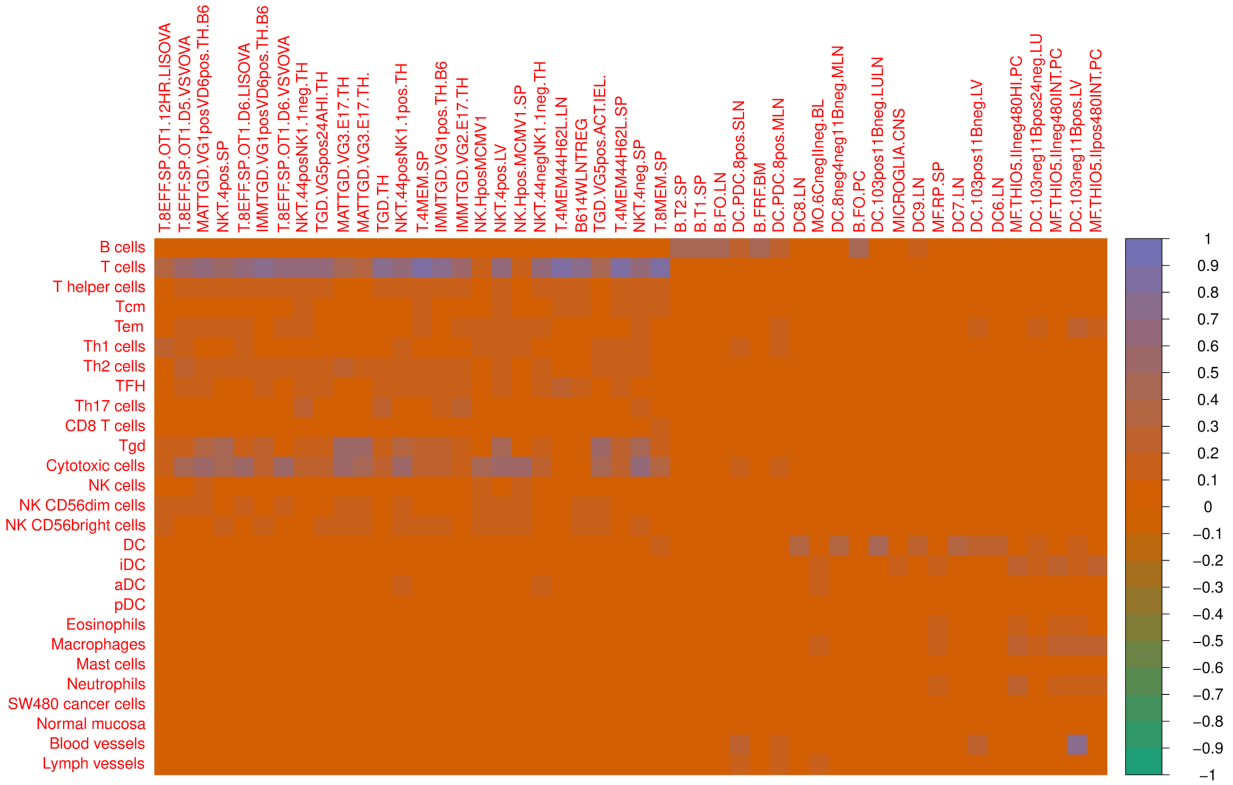


**S3. Validation of ImmGen-based weights for determining specific immune cell types in BASE for RCC samples.** ImmGen-based weights used in the BASE algorithm to determine the specific subtypes of immune cells in bulk tumor tissues were validated by examining the correlation between the ImmGen-based weights and gene expression signature sets generated by Angelova et al., 2015 for specific immune cell types.

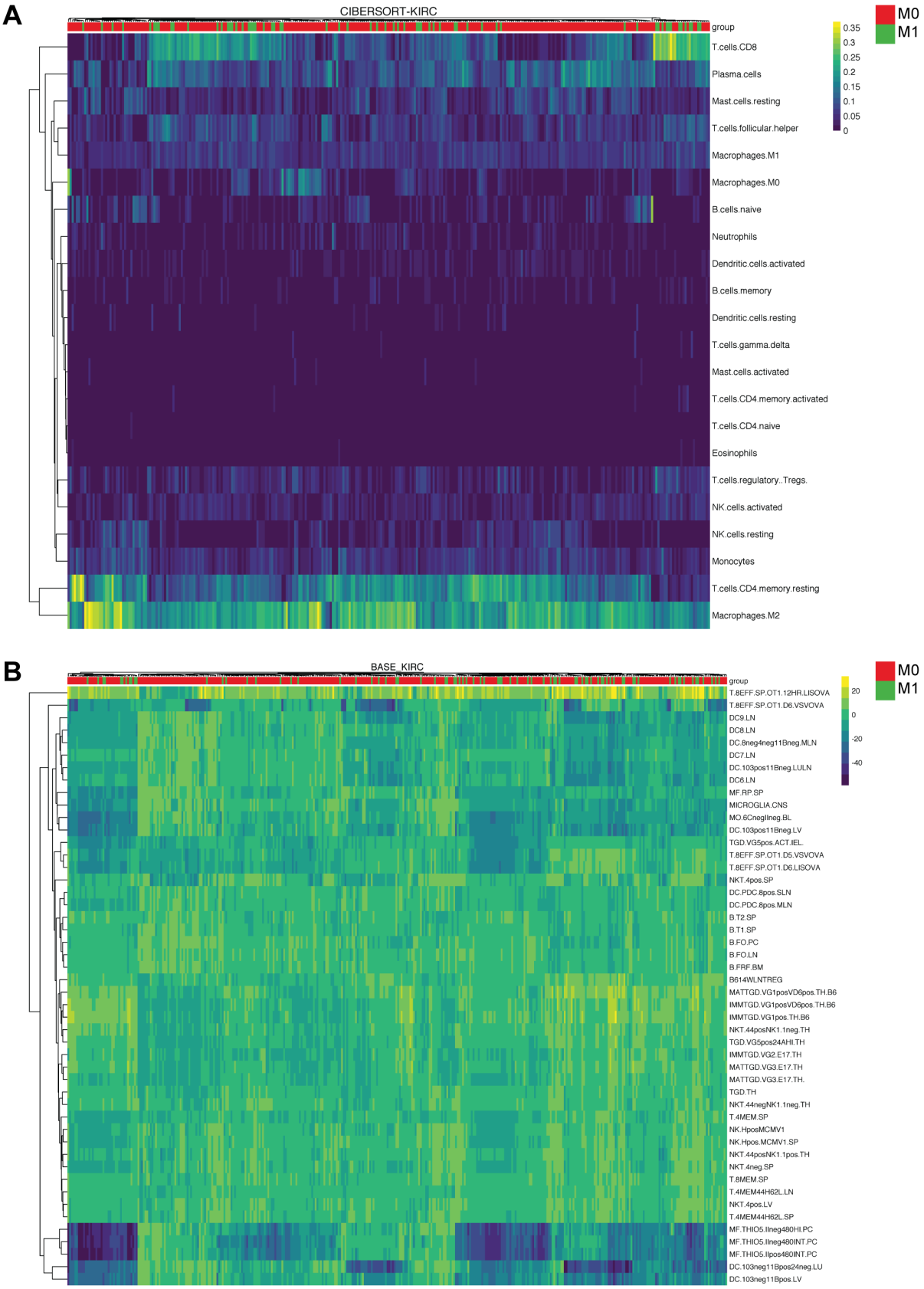


**S4. Hierarchal clustering of CIBERSORT immune fractions and BASE abundance estimates in RCC.** Immune cell scores were generated using the CIBERSORT(A) and BASE (B) algorithms for RCC. Metastatic status is noted in red (M0) and green (M1) for each tumor sample. Reference immune signatures for BASE were obtained from the ImmGen database, while CIBERSORT immune signatures were obtained from the LM22 signature noted found in Newman et al., 2016. Hierarchal clustering using the Mcquitty method was performed on 48 immune cell scores generated from BASE and on 22 immune cell fractions generated from CIBERSORT.

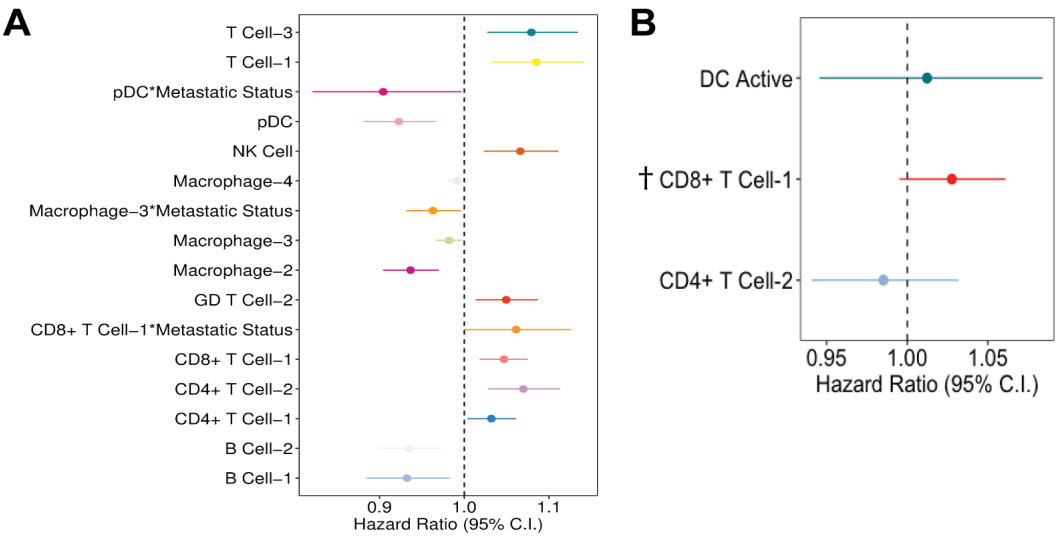


**Figure S5. Effect of immune predictors on overall survival in TCGA RCC and Miao et al., 2018 datasets.** We implemented 16 co-variate adjusted cox regression models (FDR-corrected <0.05), performed on the 13 immune predictors from LASSO and the interaction of three of the 13 immune predictors with metastatic status (CD8+ T cell-1*metastatic status trending towards significance Q =0.06), while adjusting for age and sex characteristics in each regression model (A). We also examined the effect of our immune predictors from backward selection on overall survival in the immunotherapy dataset from Mio et al., 2018 and we find CD8+ T cell-1 infiltration in pre-treatment tumors may be associated with poor overall survival in individuals treated with checkpoint blockade therapy (trending towards significance, †: p=0.06).

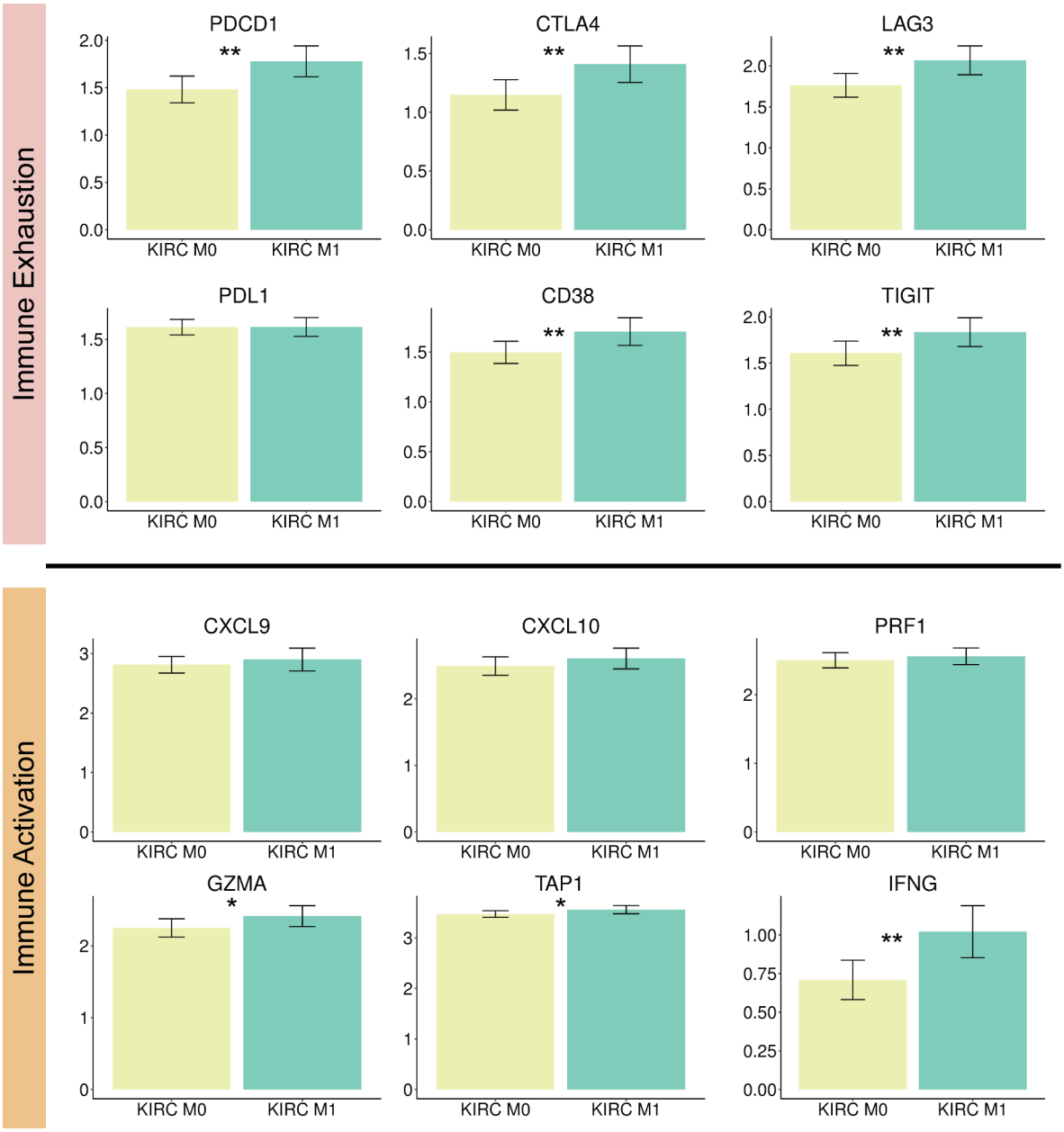


**S6. Comparison of immune activation and exhaustion marker expression in M0 and M1 tumors.** Significant differences between each M0 and M1 group are denoted by a star (*** p <0.0001, ** p<0.001, * p<0.01). Log-normalized gene expression of six major immune exhaustion markers in the TME was assessed in RCC tumors from TCGA. Expression of PDCD1, CTLA4, LAG3, and CD38 molecules was elevated in M0 vs. M1 tumors suggesting the TME of RCC M1 tumors is exhausted and an ideal candidate for immune checkpoint blockade therapy. Log-normalized gene expression of six immune activation markers in the TME was also assessed. Expression of three out of six markers was elevated in RCC M1 compared to RCC M0. CXCL9 and CXCL10 (markers of T cell recruitment), and PRF1 (marker of cytolytic activity) were not elevated in RCC M1.

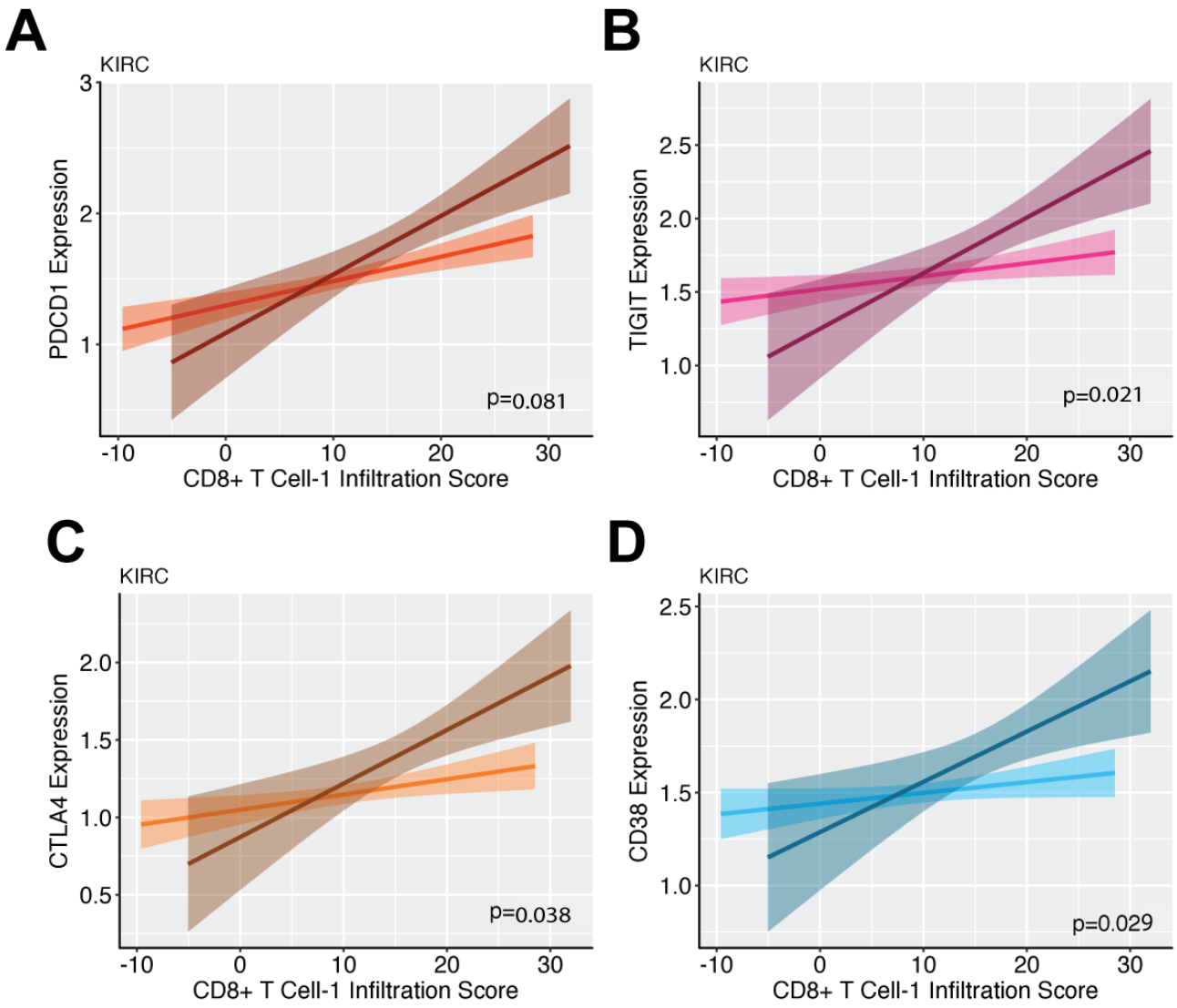


**S7. CD8+ T Cell and immune checkpoint molecule associations in M0 and M1.** Multivariate regression modeling was performed on RCC samples to determine the association between CD8+ T cell infiltration score on the expression of key immune exhaustion molecules, some of which are targets for checkpoint blockade: CD38, PDCD1, CTLA4, and TIGIT. The interaction between CD8+ T cell-1 scores and metastatic status on the gene expression of each molecule was determined for the CD8+ T cell found using BASE. Gene expression was regressed upon CD8+ T cell-1 infiltration scores, metastatic status, age, and sex, and tumor purity (measured using ABSOLUTE). Displayed are the marginal associations between gene expression and immune infiltration scores in M0 and M1 tumors, while the associated p-values are for the statistical interactor in the regression models. CD8+ T cells significantly interacted with metastatic status to determine expression of all four immune exhaustion markers.
Model: Exhaustion Marker Expression~ CD8+ T cell-1 infiltration*Metastatic Status + age + sex

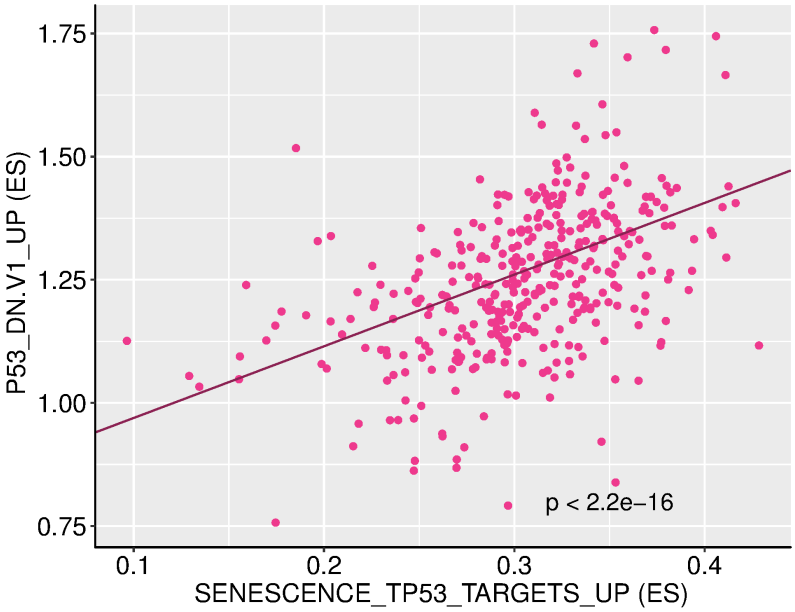


**Figure S8. Oncogenic pathway activity resulting from TP53 inactivation associates with senescence activity in TCGA cohort.** Using spearman rank correlation coefficient testing as well as regression modeling, which adjusts for metastatic disease status, we found a strong positive association between senescence activity (SENSCENCE_TP53_TARGETS_UP) and oncogenic pathway activity resulting from TP53 inactivation (P53_DN.V1_UP). These pathways share only one gene (0.52% to 3% overlap) out of 192 and 33 in P53_DN.V1_UP and SENSCENCE_TP53_TARGETS_UP respectively. These findings highlight a strong association between enrichment of TP53 inactivation induced senescence activity and enrichment of oncogenic activity resulting from TP53 inactivation.

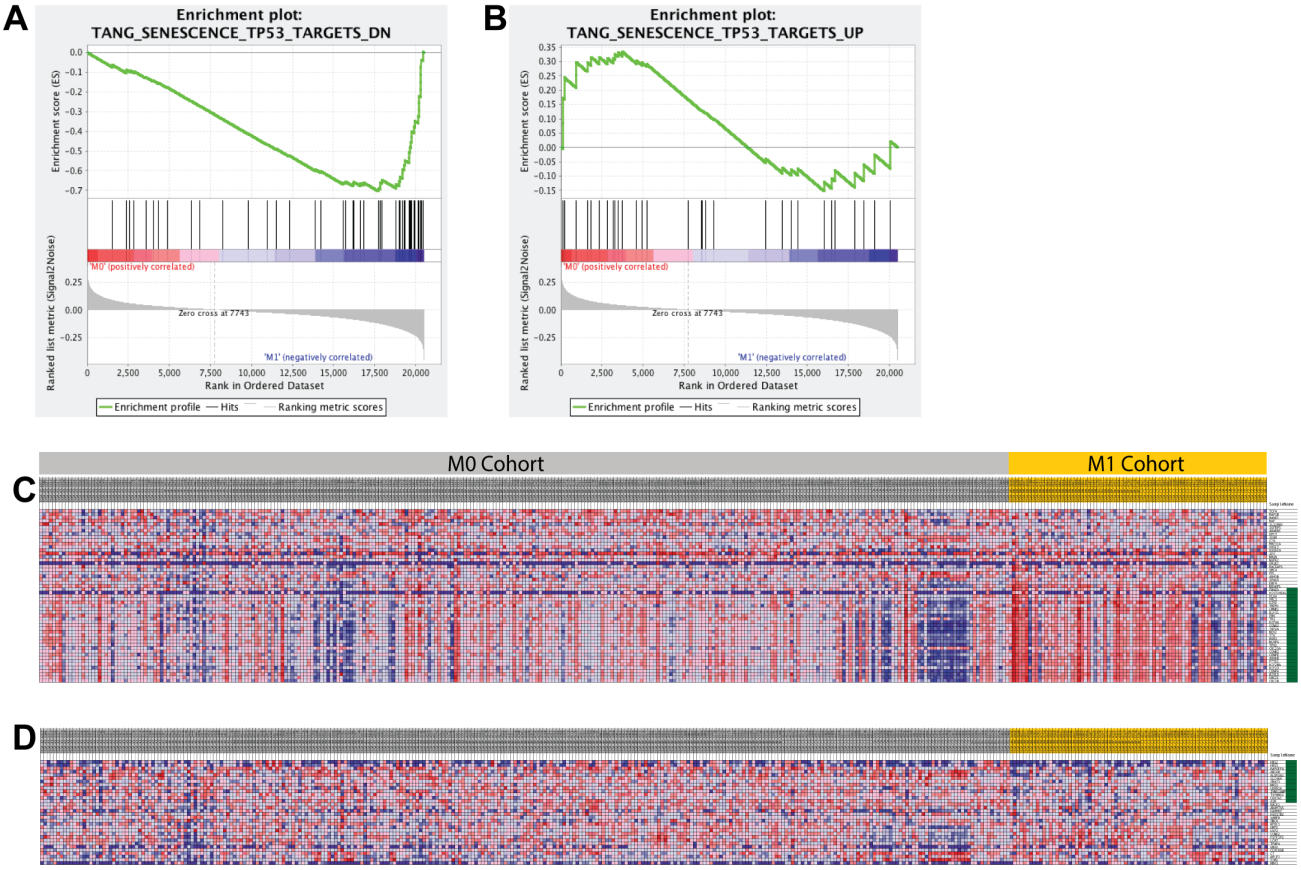


**S9. GSEA senescence enrichment results for M0 and M1 RCC TCGA comparison.** Enrichment plots for the SENESENCE_TP53_TARGETS_DN (A) and SENESENCE_TP53_TARGETS_UP (B) pathways. Differential gene expression of genes compromising the SENESENCE_TP53_TARGETS_DN (C) and SENESENCE_TP53_TARGETS_UP (D) pathways are also shown with high expression in red and low expression blue. Core genes in each pathway are denoted in green.

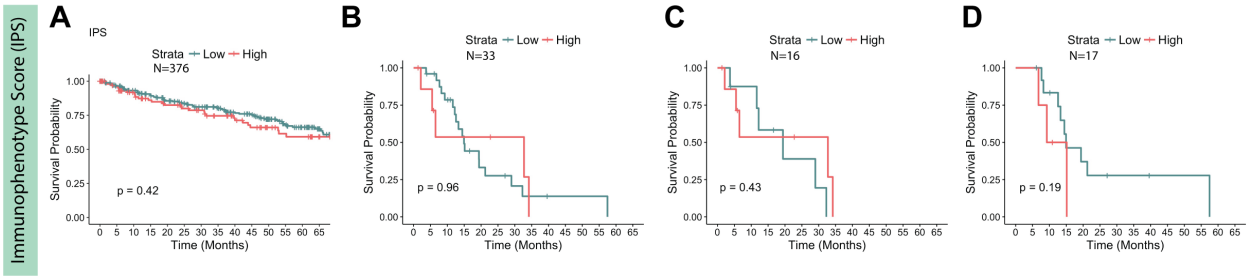


**Figure S10. High vs. low Immunophenotype score (IPS) does not predict overall survival in RCC.** Immunophenotype scores for individuals in the TCGA (A), and Miao et al., 2018 immunotherapy datasets (B-D) were generated using RNA-seq data in order to determine the association of IPS with overall survival. IPS scores were stratified into high vs. low scores for RCC based on the median score of the distribution. High vs. low IPS did not predict overall survival in the RCC datasets (A-D) as determined by log-rank test performance.

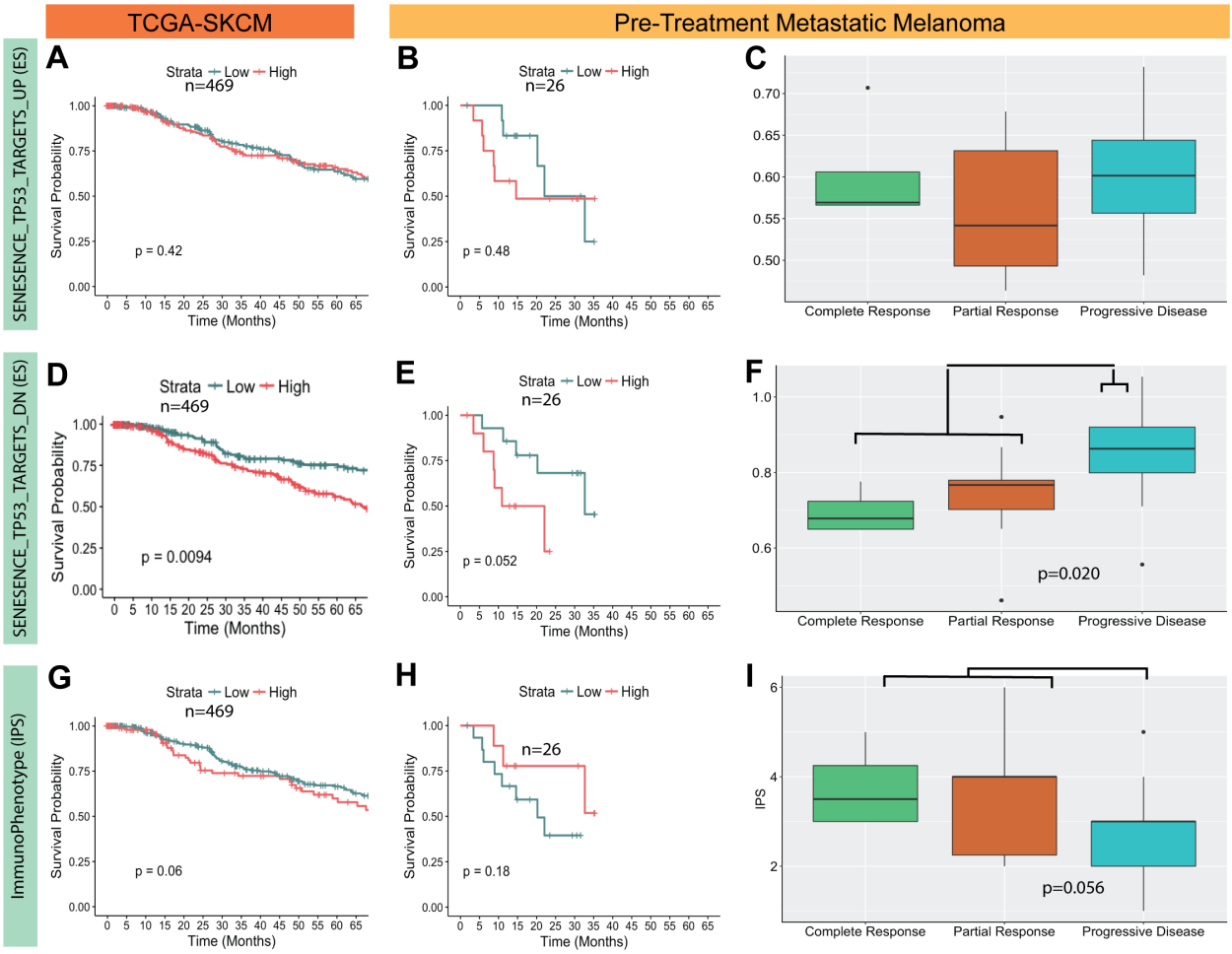


**Figure S11. SENESENCE_TP53_TARGETS_DN enrichment associates with survival and is predictive of immunotherapy outcome in metastatic melanoma.** The effect of high vs. low single-sample gene set enrichment (ssGSEA) scores for the SENESCENCE_TP53_TARGETS_DN (A) and SENESCENCE_TP53_TARGETS_UP (D) pathways in the TCGA cutaneous skin melanoma (SKCM) cohort was examined using Kaplan-Meier survival curves. High vs. low ssGSEA scores for SENESCENCE_TP53_TARGETS_DN (B) and SENESCENCE_TP53_TARGETS_UP (E) in all individuals who received anti-PD1 therapy in the Hugo et al., 2016 dataset with available RNA sequencing data on pre-treatment tumors (n=26) is also shown. The association of immunophenotype scores (IPS) with overall survival in the TCGA SKCM and the Hugo et al., 2016 anti-PD1 dataset is also shown (G-H). The cut-offs for high and low scores was set at the mean for the score distribution in each cohort. We also examined if SENESCENCE_TP53_TARGETS_DN (C) and SENESCENCE_TP53_TARGETS_UP (F) enrichment, and IPS (I) varied between the response categories in the pre-treatment tumors (n=26). Significance was assessed between responders (complete and partial response) and non-responders (progressive disease) using a Wilcoxon-rank sum test.

**Role of TP53 inactivation induced senescence in anti-PD1 therapy outcomes in metastatic melanoma.**

In this study, we show TP53-inactivation induced senescence enrichment interacts with key immune markers in renal clear cell carcinoma, and these interactions significantly influence response to immune checkpoint inhibitor therapy in stage IV renal clear cell carcinoma.

Here, we evaluated the role of TP53-inactivation induced senescence activity and its interaction with key immune markers on overall survival and response to anti-PD1 therapy in

melanoma (Fig. S10 A-F) to further support our findings on the role of senescence immune interactions in shaping the tumor immune microenvironment and response to immunotherapy treatment.

We demonstrate that SENESENCE_TP53_TARGETS_DN pathway activity is predictive of overall survival in the TCGA melanoma (SKCM) cohort (n=469) (Fig. S10 D). Next, we examined the Hugo et al., 2016 dataset, which consists of RNA-seq gene expression data on pre-treatment metastatic melanoma lesions from individuals (n=26) treated with anti-PD1 therapy (Nivolumab or pembrolizumab). Similar to the TCGA SKCM findings, we show SENESSENCE_TP53_TARGETS_DN activity is associated with worse overall survival in the Hugo et al., 2016 dataset (Fig. S10 E). Moreover, SENESSENCE_TP53_TARGETS_DN enrichment appears to differ between anti-PD1 responders and non-responders (Fig. S10 F) in pre-treatment tumors. We also found SENESSENCE_TP53_TARGETS_DN enrichment can better predict overall survival and immunotherapy response than the immunophenotype score (IPS) developed by Charoentong et al., 2017 (Fig. G-I).

Examining the interaction between SENESENCE_TP53_TARGETS_UP pathway enrichment and expression of key immune markers, such as PDCD1, PRF1, GZMA, and STING, reveals these interactions are not predictors of immunotherapy response in melanoma, with the exception of STING and SENESENCE_TP53_TARGETS_UP interactions which predict immunotherapy response as well as IPS (Table S11) based on AIC comparison. In contrast to stage IV renal clear cell carcinoma, we did not find the interaction between cGAS expression and SENESENCE_TP53_TARGETS_UP to a strong predictor of immunotherapy outcome in metastatic melanoma.

In conclusion, we demonstrate that the SENESENCE_TP53_TARGETS_DN pathway is a strong predictor of survival and immunotherapy treatment in melanoma, while SENESENCE_TP53_TARGETS_UP interactions with immunomodulatory are not strong predictors of survival or immunotherapy response, with the exception of SENESENCE_TP53_TARGETS_UP and STING interactions, which, in metastatic melanoma, predict immunotherapy response as well as IPS based on AIC comparison.

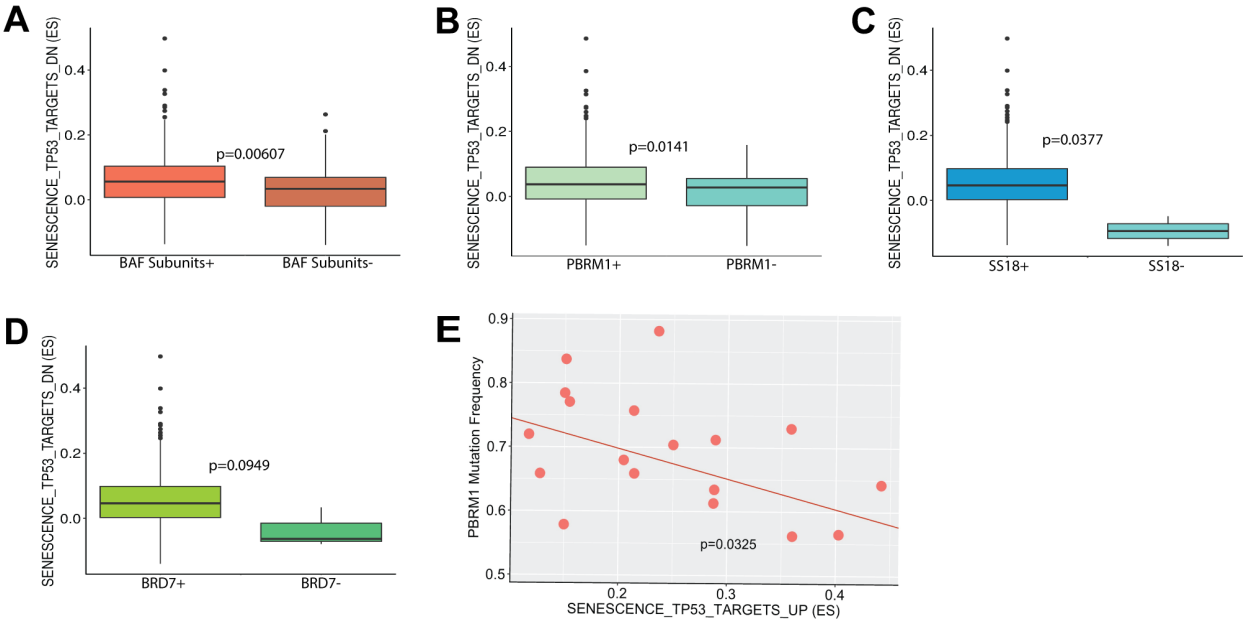


**Figure S12. Mutations in PBAF/BAF subunits associate with senescence enrichment**. We collectively examined mutations in 12 PBAF/BAF subunits which are commonly mutated in human cancer and for which we found mutations in the TCGA RCC cohort (M0 and M1 samples only). Having a mutation in any of the 12 PBAF/BAF subunits associates with reduced SENESCENCE_TP53_TARGETS_DN enrichment based on Wilcox rank sum test (A). Furthermore, having mutations in three PBAF/BAF subunits, PBRM1, SS18, and BRD7, individually associates with lower SENESCENCE_TP53_TARGETS_DN enrichment. We show the p-values associated with these mutations (not FDR-corrected) based on performance in Wilcox rank sum test (B-D). We also determined if PBRM1 mutation frequency in the immunotherapy cohort associated with SENESENCE_TP53_TARGETS_UP pathway enrichment using regression modeling, which adjusted for age, sex, cohort status (E).

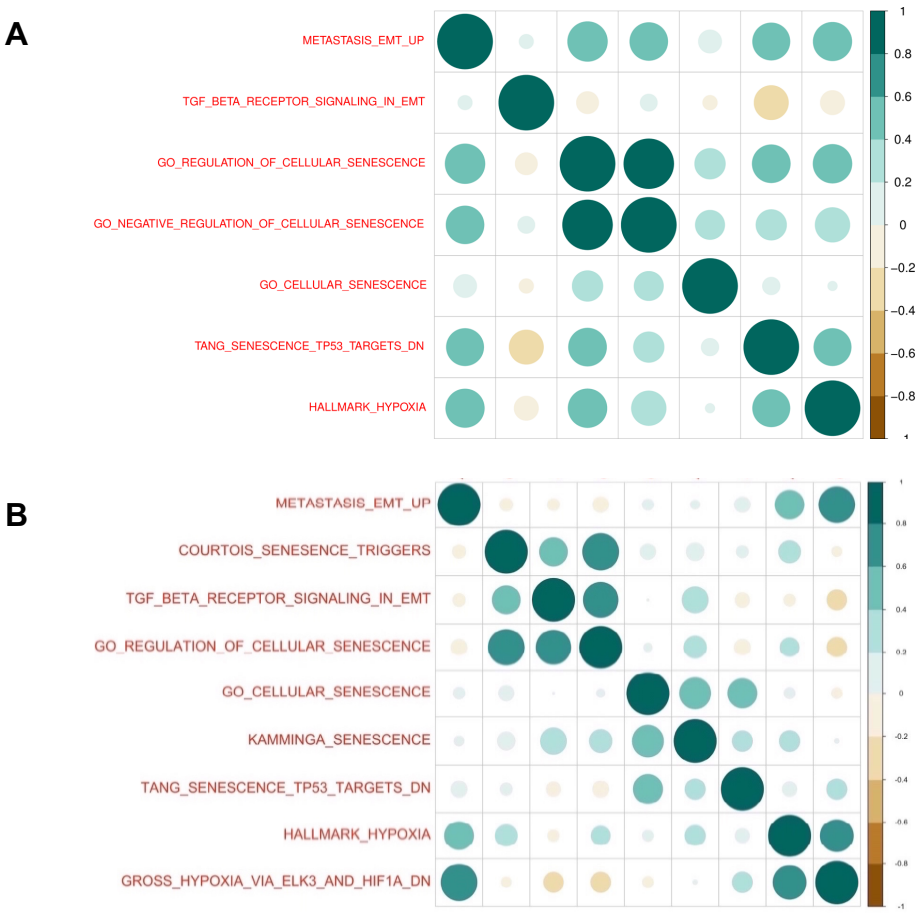


**S13. Examining the relationship between senescence, hypoxia, and metastasis pathways in RCC tumors.** Correlation plot displaying the correlation between the four enriched senescence pathways found in RCC M1 tumors and hypoxia and EMT transition pathways in TCGA RCC (M0+M1) dataset (A) as well as the renal cell carcinoma immunotherapy dataset (B)